Equilibrium and real-time properties of the spin correlation function in the two-impurity Kondo model

Benedikt Lechtenberg[1] and Frithjof B. Anders[2]
[1]*Department of Physics, Kyoto University, Kyoto 606-8502, Japan*
[2]*Lehrstuhl für Theoretische Physik II, Technische Universität Dortmund, 44221 Dortmund,Germany*

(Received 11 May 2018; revised manuscript received 20 June 2018; published 6 July 2018)

We investigate the equilibrium and real-time properties of the spin-correlation function $\langle \vec{S}_1 \vec{S}_2 \rangle$ in the two-impurity Kondo model for different distances R between the two-impurity spins. It is shown that the competition between the Ruderman-Kittel-Kasuya-Yosida (RKKY) interaction and the Kondo effect governs the amplitude of $\langle \vec{S}_1 \vec{S}_2 \rangle$. For distances R exceeding the Kondo length scale, the Kondo effect also has a profound effect on the sign of the correlation function. For ferromagnetic Heisenberg couplings J between the impurities and the conduction band, the Kondo effect is absent and the correlation function only decays for distances beyond a certain length scale introduced by finite temperature. The real-time dynamics after a sudden quench of the system reveals that correlations propagate through the conduction band with Fermi velocity. We identify two distinct timescales for the long-time behavior, which reflects that for small J the system is driven by the RKKY interaction while for large J the Kondo effect dominates. Interestingly, we find that at certain distances a one-dimensional dispersion obeying $\epsilon(k) = \epsilon(-k)$ may lead to a local parity conservation of the impurities such that $\langle \vec{S}_1 \vec{S}_2 \rangle$ becomes a conserved quantity for long times and does not decay to its equilibrium value.

DOI: 10.1103/PhysRevB.98.035109

I. INTRODUCTION

Quantum impurity systems are promising candidates for the realization of solid-state-based quantum bits [1–5]. The perspective of combining traditional electronics with novel spintronics devices leads to an intense research of controlling and switching magnetic properties of such systems. Magnetic properties of adatoms on surfaces [6–11] or magnetic molecules [12–19] might serve as the smallest building blocks for such devices.

From a theoretical perspective, the two-impurity Kondo model (TIKM) [20–24] constitutes an important but simple system which embodies the competition of interactions between two localized magnetic moments with those between the impurities and the conduction band. The TIKM has been viewed as a paradigm model for the formation of two different singlet phases separated by a quantum critical point (QCP): a Ruderman-Kittel-Kasuya-Yosida (RKKY) [25–27] interaction induced singlet and a Kondo singlet [28]. This quantum critical point investigated by Jones and Varma (see Refs. [20,21,29]), however, turned out to be unstable against particle-hole (PH) symmetry breaking [24]. The two different singlet phases are adiabatically connected by a continuous variation of the scattering phase. This led to the conclusion that for finite distances between the impurities no QCP exists, and the original finding is just a consequence of unphysical approximations [23] which is generically replaced by a crossover regime [30]. Only recently, it has been shown [31] that for certain dispersions and distances between the impurities the TIKM exhibits a QCP between two orthogonal ground states with different degeneracy.

In this paper, we examine the equilibrium as well as nonequilibrium properties of the spin-correlation function $\langle \vec{S}_1 \vec{S}_2 \rangle(R)$ for different distances R between both impurity spins using the numerical renormalization group (NRG) [32,33] and its extension to the nonequilibrium dynamics, the time-dependent NRG (TD-NRG) [34,35]. Previously, the spatial dependence of the equilibrium properties has been mainly studied using a simplified density of states (DOS) [20,21,36] that suppresses the antiferromagnetic (AFM) correlations [24]. In this paper, we include the full energy dependency of the even- and odd-parity conduction-band DOSs that properly encode the ferromagnetic (FM) as well as the antiferromagnetic contributions to the RKKY interaction. This approach generates the correct RKKY interaction and does not require adding an artificial spin-spin interaction to account for this term [20,21,36].

In order to set the stage for the investigation of the nonequilibrium quench dynamics, we present results for the impurity spin-spin-correlation function $\langle \vec{S}_1 \vec{S}_2 \rangle(R)$. For an isotropic dispersion in one dimension, we find that the amplitude of $\langle \vec{S}_1 \vec{S}_2 \rangle(R)$ is completely governed by the ratio between the distance of the impurities and the Kondo length scale R/ξ_K. $\xi_K = v_F/T_K$ is often referred to as the size of the Kondo screening cloud where v_F denotes the Fermi velocity of the metallic host and T_K denotes the Kondo temperature. For small distances $R < \xi_K$ and vanishing temperature, steplike oscillations between ferromagnetic and antiferromagnetic correlations can be observed for $\langle \vec{S}_1 \vec{S}_2 \rangle(R)$ due to the RKKY interaction. Interestingly, at large distances $R \geqslant \xi_K$ the ferromagnetic correlations vanish and only small antiferromagnetic correlations between the impurities are found. These weak antiferromagnetic correlations are related to the PH symmetry breaking in the two parity channels and vanish for $R \to \infty$.

For a ferromagnetic coupling between the impurities and the conduction band, the Kondo effect is absent, and a constant amplitude for the correlations is observed at zero temperature even for $R \to \infty$. A finite temperature introduces a new length scale beyond which correlations are exponentially suppressed.

The time dynamics of the correlation function $\langle \vec{S}_1 \vec{S}_2 \rangle(R,t)$ is examined after a quench in the coupling strength between the impurities and the conduction band, starting from initially decoupled impurities. Experimentally, such quenches can be realized with strong laser light [37]. We have identified two distinct timescales characterizing the long-time behavior: The RKKY interaction drives the dynamics for small Kondo coupling whereas a timescale $\propto 1/\sqrt{T_K}$ indicates that the physics is dominated by the Kondo effect at large Kondo coupling.

The correlation function approaches its equilibrium value in the steady state for most distances. For special R, however, it remains almost constant although the RKKY interaction reaches a ferromagnetic maximum for those distances. Focusing on a dispersion of an inversion symmetric one-dimensional (1D) lattice, parity conduction-band states decouple from the impurities at low temperatures, thus enforcing a local impurity parity conservation such that $\langle \vec{S}_1 \vec{S}_2 \rangle$ becomes a conserved quantity for long times.

We combined the time-dependent correlation functions for different but fixed distances into a two-dimensional (2D) spatial-temporal picture of the real-time dynamics. It allows for better visualization of the the propagation of correlations. Starting from a distance around $k_F R/\pi = 0.5$ a ferromagnetic correlation emerges which afterwards propagates with the Fermi velocity v_F, defining a light cone [38,39], through such a fictitious two-impurity Kondo system with variable impurity distance R.

II. MODEL AND METHODS

A. Mapping the model onto an effective two-band model

While Wilson's original NRG approach [32] was only designed to solve the thermodynamics of one localized impurity, the NRG was later successfully extended by Jones and Varma (see Refs. [12,20,21,24,36,39,40]) to two impurities separated by a distance R. For this purpose the conduction band is divided into two bands, one with even-parity and one with odd-parity symmetry, the effective DOSs of which incorporated the spatial extension. In the following, we briefly summarize this procedure for the TIKM.

The Hamiltonian of the TIKM can be separated into three parts $H = H_c + H_{\rm int} + H_d$. H_c contains the conduction band $H_c = \sum_{\vec{k},\sigma} \epsilon_{\vec{k}} c^\dagger_{\vec{k},\sigma} c_{\vec{k},\sigma}$ where $c^\dagger_{\vec{k},\sigma}$ creates an electron with spin σ and momentum $\vec{k}$. The interaction between the conduction band and the impurities is given by

$$H_{\rm int} = J[\vec{S}_1 \vec{s}_c(\vec{R}_1) + \vec{S}_2 \vec{s}_c(\vec{R}_2)], \tag{1}$$

where the impurity $\vec{S}_i$ located at position $\vec{R}_i$ is coupled via the effective Heisenberg coupling J to the unit-cell volume averaged conduction electron spin $\vec{s}_c(\vec{r}) = V_u \vec{s}(\vec{r})$. Here, $\vec{s}(\vec{r})$ is the conduction-band spin density operator expanded in planar waves:

$$\vec{s}(\vec{r}) = \frac{1}{2}\frac{1}{N V_u} \sum_{\sigma\sigma'} \sum_{\vec{k}\vec{k}'} c^\dagger_{\vec{k}\sigma} [\vec{\sigma}]_{\sigma\sigma'} c_{\vec{k}'\sigma'} e^{i(\vec{k}'-\vec{k})\vec{r}}, \tag{2}$$

with N being the number of unit cells in the volume V, $V_u = V/N$ the volume of such a unit cell, $\vec{k}$ a momentum vector, and $\vec{\sigma}$ a vector of the Pauli matrices. In the following, we set the origin of the coordinate system in the middle of the two impurities such that $\vec{R}_1 = \vec{R}/2$ and $\vec{R}_2 = -\vec{R}/2$.

H_D comprises all contribution acting only on the impurities

$$H_d = K \vec{S}_1 \vec{S}_2, \tag{3}$$

with the direct Heisenberg interaction K between two-impurity spins. Unless stated otherwise, we use $K = 0$ throughout this paper.

Instead, the correlations between the two-impurity spins are caused by the indirect Heisenberg interaction $K_{\rm RKKY} \propto J^2$ which is mediated by the conduction-band electrons [25–27].

Exploiting the symmetry [12,20,21,24,36,39–41], the conduction electron band is mapped onto the two distance and energy dependent orthogonal even-parity (e) and odd-parity (o) eigenstate field operators:

$$c_{\sigma,e/o}(\epsilon) = \sum_{\vec{k}} \delta(\epsilon - \epsilon_{\vec{k}}) c_{\vec{k},\sigma} \frac{(e^{+i\vec{k}\vec{R}/2} \pm e^{-i\vec{k}\vec{R}/2})}{N_{e/o}(\epsilon,\vec{R})\sqrt{N\rho_c(\epsilon)}}. \tag{4}$$

Here $\rho_c(\epsilon)$ is the DOS of the original conduction band and the dimensionless normalization functions are defined as

$$N_e^2(\epsilon,\vec{R}) = \frac{4}{N\rho_c(\epsilon)} \sum_{\vec{k}} \delta(\epsilon - \epsilon_{\vec{k}}) \cos^2\left(\frac{\vec{k}\vec{R}}{2}\right), \tag{5a}$$

$$N_o^2(\epsilon,\vec{R}) = \frac{4}{N\rho_c(\epsilon)} \sum_{\vec{k}} \delta(\epsilon - \epsilon_{\vec{k}}) \sin^2\left(\frac{\vec{k}\vec{R}}{2}\right) \tag{5b}$$

such that $c_{\sigma,e/o}(\epsilon)$ fulfill the standard anticommutator relation $\{c_{\sigma,p}(\epsilon), c^\dagger_{\sigma',p'}(\epsilon')\} = \delta_{\sigma,\sigma'}\delta_{p,p'}\delta(\epsilon - \epsilon')$. With these even- and odd-parity conduction-band states the interaction part of the Hamiltonian reads

$$\begin{aligned} H_{\rm int} = \frac{J}{8} \int\int d\epsilon\, d\epsilon' \sqrt{\rho_c(\epsilon)\rho_c(\epsilon')} \sum_{\sigma\sigma'} \vec{\sigma}_{\sigma\sigma'} \\ \times \Big\{ (\vec{S}_1 + \vec{S}_2) \sum_p [N_p(\epsilon,R) N_p(\epsilon',R) c^\dagger_{\sigma,p}(\epsilon) c_{\sigma',p}(\epsilon')] \\ + (\vec{S}_1 - \vec{S}_2) N_e(\epsilon,R) N_o(\epsilon',R) [c^\dagger_{\sigma,e}(\epsilon) c_{\sigma',o}(\epsilon') + \text{H.c.}] \Big\}. \end{aligned} \tag{6}$$

It is important to note that due to the energy dependent factors $N_p(\epsilon,R)$ the model will generally be particle-hole asymmetric even if the original conduction band and, therefore, the original DOS $\rho_c(\epsilon)$ are particle-hole symmetric. For $N_e(\epsilon,R) \neq N_o(\epsilon,R)$ this asymmetry will generate potential scattering terms that are different for the even and odd conduction bands and lead to the destruction of the Jones and Varma QCP (see Refs. [24,42]).

Up until now we have not specified the dispersion of the conduction band. Unless stated otherwise, we will use a 1D

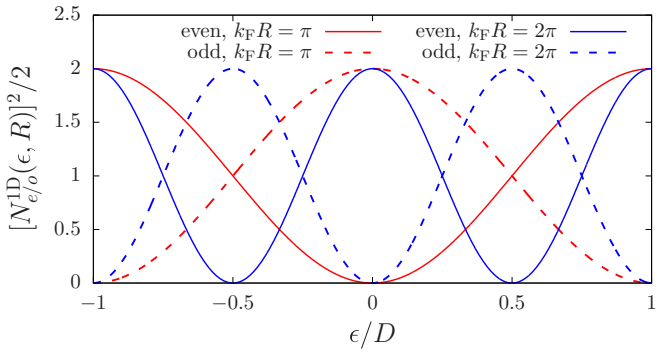

FIG. 1. Normalization functions of Eq. (7) for a linear dispersion in one dimension for two different distances $k_F R = \pi$ (red) and $k_F R = 2\pi$ (blue). For these distances either the even (solid) or the odd (dashed) normalization function exhibits a pseudogap at $\epsilon = 0$.

linear dispersion $\epsilon(k) = v_F(|k| - k_F)$ throughout this paper which yields for the normalization functions [39,40]

$$\left[N^{1D}_{e/o}(\epsilon, R)\right]^2 \rho_c(\epsilon) = 2\rho_c(\epsilon)\left\{1 \pm \cos\left[k_F R\left(1 + \frac{\epsilon}{D}\right)\right]\right\}, \tag{7}$$

with the half bandwidth $D = v_F k_F$. $[N^{1D}_{e/o}(\epsilon, R)]^2$ are plotted for the two different distances $k_F R/\pi = 1$ and 2 in Fig. 1. Note that one of the normalization functions exhibits a pseudogap at the Fermi energy $\epsilon = 0$ for distances $k_F R/\pi = n$, with $n = 0, 1, 2, \ldots$ as a consequence of the dispersion $\epsilon(k) = \epsilon(-k)$ [31] employed here. This can also be seen from the definitions in Eq. (7). It has been pointed out that the absence of the screening in one of the parity channels leads to the breakdown of the two-stage Kondo screening process and the emergence of a new kind of quantum critical point in the TIKM [31]. This has also a profound effect on the time dynamics of the TIKM.

In addition to the emergence of the pseudogap, both normalization functions are particle-hole symmetric for these special distances and, thus, lead to a completely particle-hole symmetric model.

B. Nonequilibrium dynamics and the TD-NRG

In order to calculate the real-time dynamics of the TIKM, we employ the TD-NRG, which is an extension of the standard NRG.

The TD-NRG [34,35] is designed to calculate the full nonequilibrium dynamics of a quantum impurity system after a sudden quench: $H(t) = H_0\Theta(-t) + H_f\Theta(t)$.

For this purpose, the initial state of the system is described by the density operator

$$\rho_0 = \frac{e^{-\beta H_0}}{\mathrm{Tr}[e^{-\beta H_0}]}, \tag{8}$$

until at time $t = 0$ the system is suddenly quenched. Afterwards, the system is characterized by the Hamiltonian H_f and the time evolution of the density operator is given by

$$\rho(t \geqslant 0) = e^{-itH_f}\rho_0 e^{itH_f}. \tag{9}$$

By means of the TD-NRG the time-dependent expectation value $O(t)$ of a general local operator O should be calculated. In this paper, the local operator is given by the spin-correlation function of both impurities $O = \langle \vec{S}_1 \vec{S}_2 \rangle$.

The time evolution of such local operators can be written as [34,35]

$$\langle O \rangle(t) = \sum_m^N \sum_{r,s}^{\mathrm{trun}} e^{it(E^m_r - E^m_s)} O^m_{r,s} \rho^{\mathrm{red}}_{s,r}(m), \tag{10}$$

where E^m_r and E^m_s are the NRG eigenenergies of the Hamiltonian H_f at iteration $m \leqslant N$, $O^m_{r,s}$ is the matrix representation of O at that iteration, and $\rho^{\mathrm{red}}_{s,r}(m)$ is the reduced density matrix defined as

$$\rho^{\mathrm{red}}_{s,r}(m) = \sum_e \langle s, e; m|\rho_0|r, e; m\rangle, \tag{11}$$

in which the environment is traced out. In Eq. (10) the restricted sums over r and s require that at least one of these states is discarded at iteration m. The temperature $T_N \propto \Lambda^{-N/2}$ of the TD-NRG calculation is defined by the length of the NRG Wilson chain N and enters Eq. (8). Here, $\Lambda > 1$ denotes the Wilson discretization parameter.

The TD-NRG comprises two simultaneous NRG runs: one for the initial Hamiltonian H_0 in order to compute the initial density operator ρ_0 of the system in Eq. (8) and one for H_f to obtain the approximate eigenbasis governing the time evolution in Eq. (10).

This approach has also been extended to multiple quenches [43], time evolution of spectral functions [44], and steady-state currents at finite bias [45–47]. The only error of this method originates from the representation of the bath continuum by a finite-size Wilson chain [32]. This error is essentially well understood [48,49] and may lead to artificial oscillations and slight deviations of the long time value from the exact result. These can be reduced by using an increased number of NRG z-tricks [50].

III. EQUILIBRIUM

A. Antiferromagnetic coupling J

Two characteristic length scales have been identified [39,40] in the TIKM with an antiferromagnetic J for $T = 0$: the inverse Fermi momentum $1/k_F$ and the Kondo length scale $\xi_K = v_F/T_K$ with the Kondo temperature $T_K = \sqrt{\rho J}\, e^{-1/\rho J}$. The length scale $1/k_F$ defines the oscillations of the RKKY interaction and its envelope. As ξ_K changes exponentially with the Kondo coupling J, we use different J to examine the different distances $R < \xi_K$ and $R > \xi_K$.

The impurity spin-correlation function $\langle \vec{S}_1 \vec{S}_2 \rangle(R)$ is shown in conjunction with the RKKY interaction (dashed line) in Fig. 2(a) for different couplings J. For $R \ll \xi_K$ (small Kondo couplings J) one can clearly observe oscillations between ferromagnetic and antiferromagnetic correlations caused by the RKKY interaction. For an effective ferromagnetic RKKY interaction, the impurity spins align parallel while for an antiferromagnetic interaction they align antiparallel.

For these small distances $R \ll \xi_K$ the impurity spins are located inside the respective screening cloud of the other impurity and are not completely screened by the conduction electrons. Therefore, the Kondo effect has almost no effect on $\langle \vec{S}_1 \vec{S}_2 \rangle(R)$, which can be seen by a comparison with Fig. 4(a)

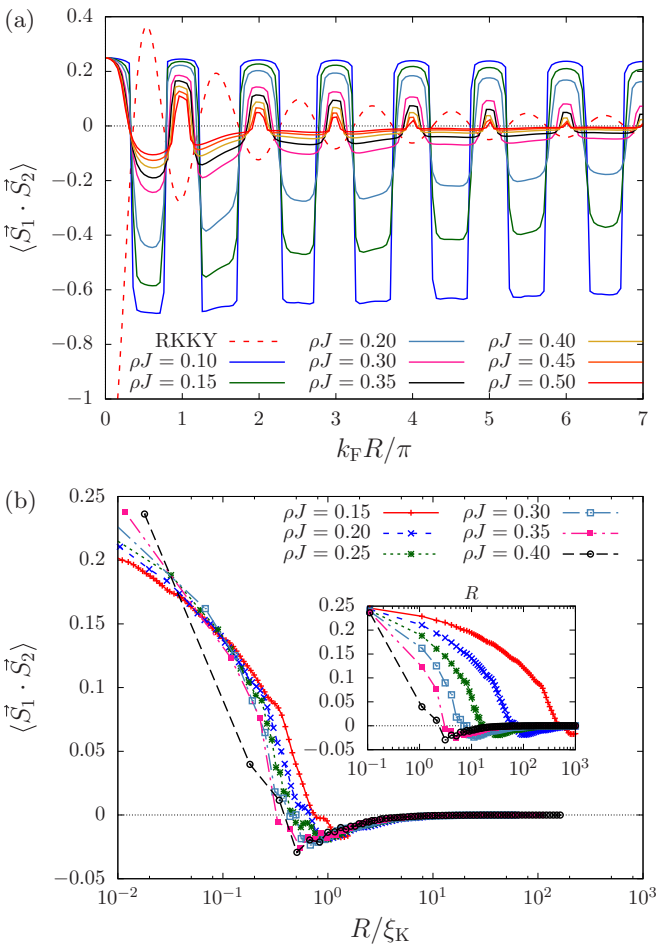

FIG. 2. (a) The $\langle \vec{S}_1 \vec{S}_2 \rangle(R)$ correlation function plotted against the distance $k_F R/\pi$ for different antiferromagnetic couplings J. The red dashed line depicts the 1D RKKY interaction $\propto 1/R$ in arbitrary units. Note that for distances $R \approx \xi_K$ (large J values) the ferromagnetic correlations around $k_F R/\pi = n$ begin to vanish. For $R \gg \xi_K$ only at exactly $k_F R/\pi = n$ ferromagnetic correlations persist. (b) Correlation function for the distances $k_F R/\pi = (n + 0.11)$ and different couplings J plotted against the rescaled distance R/ξ_K. The inset shows the same data vs the distance R.

showing $\langle \vec{S}_1 \vec{S}_2 \rangle(R)$ for ferromagnetic couplings J where the Kondo effect is absent.

Note that $\langle \vec{S}_1 \vec{S}_2 \rangle(R)$ does not decay but instead exhibits steplike oscillations with a constant amplitude since it reflects the ground-state properties of two free impurity spins which are coupled via a Heisenberg interaction. Even for an infinitesimal small effective Heisenberg interaction between the impurity spins, the spins align completely parallel or antiparallel at $T = 0$.

This behavior is modified for larger couplings J, where $R \ll \xi_K$ is not valid anymore due to an increasing Kondo temperature. Upon lowering the temperatures, the spins begin to align parallel or antiparallel until the Kondo temperature T_K is reached, at which the impurities are screened by the conduction electrons and, hence, the correlation function does not change anymore. The exact value of the correlation function depends on the ratio between the RKKY interaction and the Kondo temperature K_{RKKY}/T_K [20].

Furthermore, one should note that when the distance approaches the Kondo length scale, $R \sim \xi_K$, large J and R in Fig. 2(a), the Kondo effect leads to a drastic departure from the conventional RKKY interaction [51]. While for small J and R the position of the sign change of the RKKY interaction agrees with the position of the sign change of the correlation function, the latter is shifted towards the integer distances $k_F R/\pi = n$ with increasing coupling J and distance R. The interval in the vicinity of the distances $k_F R/\pi = n$ where we observe ferromagnetic correlation, therefore, shrinks and antiferromagnetic correlations between the impurity spins emerge instead [22].

Since ξ_K exponentially depends on the Kondo coupling J, the precise distance R at which the ferromagnetic correlations disappear is also J dependent. Therefore, one almost only observes antiferromagnetic correlations between the impurities for $R \gg \xi_K$.

In order to review the influence of the Kondo effect on the ferromagnetic correlations, we calculated $\langle \vec{S}_1 \vec{S}_2 \rangle(R)$ at the distances $k_F R/\pi = (n + 0.11)$ where we expect a finite FM RKKY interaction. The results are shown in Fig. 2(b) plotted as a function of the rescaled distance R/ξ_K and as a function of R in the inset. The crossover from FM to AFM is governed by the Kondo effect and occurs once the distance exceeds $R \sim 0.53\xi_K$.

Based on the observed universality, we can understand this surprising sign change of the spin-spin-correlation function within the strong-coupling limit. For $J \to \infty$, a Kondo singlet is formed locally at each impurity site, and the local conduction-band electron is antiparallel to the local spin. In this case, the system consists of two Kondo singlets which are decoupled from the remaining Fermi sea with two missing electrons. In the generic case, however, the two bound states in the even-odd basis are subject to the potential scattering terms emerging from the particle-hole asymmetry (see Sec. II A). These scattering terms are different for the even and odd conduction-band channel [24,52] and, hence, generate a hopping term between the bound states in the real-space basis.

This hopping term evokes an antiferromagnetic interaction so that the two bound conduction electron spins arrange in opposite orientation inducing an AF correlation between the impurity spins as observed in Fig. 2(b) for $R/\xi_K > 1$.

A word is in order to justify the choice $k_F R/\pi = (n + 0.11)$ as generic distance. $k_F R/\pi = n$ leads to a different physics [31] for a linear dispersion in one dimension considered here for two reasons: At first, one of the two parity conduction bands develops a pseudogap DOS at low temperatures, as depicted in Fig. 1, and does not participate in the screening any more. Second, at $k_F R/\pi = n$ the system is perfectly particle-hole symmetric and the above-mentioned additional hopping term between the bound conduction electrons does not appear. Consequently, the system is equivalent to the physics at $R = 0$ [12] for these distances and ferromagnetic correlations remain for all integers n.

A similar behavior has also been observed in the single impurity Kondo model (SIKM) for the correlation function $\langle \vec{S}\vec{s}(R) \rangle$ which measures the correlations between the impurity spin and the spin density of the conduction band in distance R to the impurity [39]. The ferromagnetic correlations located at $k_F R/\pi = (n + 0.5)$ vanish for distances $R > \xi_K$ and instead

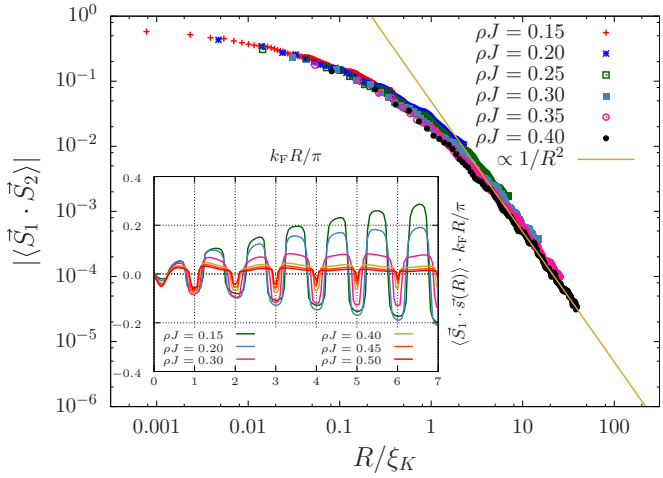

FIG. 3. The envelope $|\langle \vec{S}_1 \vec{S}_2 \rangle(R)|$ of the impurity spin-correlation function on a double logarithmic scale plotted against the rescaled distance R/ξ_K. The rescaling leads to a universal behavior. For large distances $R \gg \xi_K$ a $1/R^2$ decrease is observed. The inset shows the correlation function $\langle \vec{S}\vec{s}(R) \rangle$ between an impurity spin $\vec{S}$ and the conduction-band spin density $\vec{s}(R)$ at distance R from the impurity.

also antiferromagnetic correlations appear in accordance with theoretical predictions [53,54].

The inset of Fig. 3 shows the same correlation function $\langle \vec{S}\vec{s}(R) \rangle$ for the TIKM measuring the correlation between an impurity spin and the conduction-band spin density at the position of the second impurity located a distance R from the first impurity. To counteract the decay, the correlation function has been rescaled with the distance R for a better prospect. In comparison to the correlation function for the SIKM, the second impurity leads to a $\pi/2$ phase shift such that now the antiferromagnetic correlations around $k_F R/\pi = n$ instead of the ferromagnetic ones around $k_F R/\pi = (n + 0.5)$ vanish. Consequently, the ferromagnetic correlations between the impurity spins $\langle \vec{S}_1 \vec{S}_2 \rangle(R)$ at the distances $k_F R/\pi = n$ also have to vanish since the RKKY interaction between the impurity spins is mediated by the conduction band.

Figure 3 depicts the envelope of $\langle \vec{S}_1 \vec{S}_2 \rangle(R)$ measured at the distances $k_F R/\pi = (n + 0.5)$. The universal behavior of the envelope function is revealed by plotting the data as a function of the dimensionless distance R/ξ_K. This shows that the amplitude of the correlation function is completely governed by the distance dependent RKKY interaction and the Kondo effect. For large distances $R \gg \xi_K$ a $\propto 1/R^2$ behavior, indicated by the solid line, is observed. At these large distances the impurities are located outside of the Kondo screening cloud of the respective other almost completely screened impurity, therefore the $\propto 1/R$ decay of the RKKY interaction in one dimension is enhanced to a $\propto 1/R^2$ decay. The same $\propto 1/R^2$ behavior for $R \gg \xi_K$ has also been found for the correlation between an impurity spin and the conduction-band spin density $\langle \vec{S}\vec{s}(R) \rangle$ in the SIKM [39].

B. Ferromagnetic coupling J and finite temperatures

So far, we have only investigated the TIKM for an antiferromagnetic coupling J where the Kondo effect is present. We now extend our discussion also to ferromagnetic J.

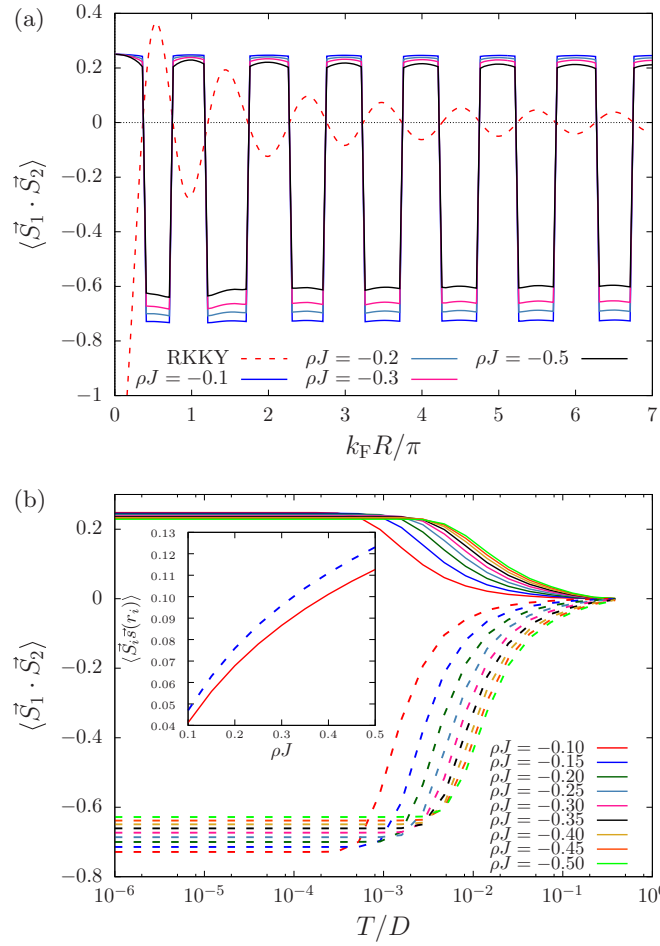

FIG. 4. (a) The $\langle \vec{S}_1 \vec{S}_2 \rangle(R)$ correlation function vs the distance $k_F R/\pi$ for different ferromagnetic couplings J. The red dashed lines depicts the 1D RKKY interaction $\propto 1/R$ in arbitrary units. (b) Temperature-dependent correlation function for different couplings and the two different distances $k_F R/\pi = 1.0$ (solid lines), where the RKKY interaction is ferromagnetic, and $k_F R/\pi = 0.5$ (dashed lines), where the RKKY interaction is antiferromagnetic. The inset shows the fixed-point value of the correlation between an impurity spin and the spin density of the conduction electrons at the position of this impurity $\langle \vec{S}_i \vec{s}(r_i) \rangle$ for different couplings J and the two distances $k_F R/\pi = 1.0$ (red solid line) and $k_F R/\pi = 0.5$ (blue dashed line).

The correlation function $\langle \vec{S}_1 \vec{S}_2 \rangle(R)$ for ferromagnetic couplings as well as the RKKY interaction (dashed line) is depicted in Fig. 4(a). Since the Kondo effect is absent, there is no screening of the local moments with increasing J in contrast to AFM J shown in Fig. 2(a). The correlation function preserves its steplike oscillations even for very large ferromagnetic couplings.

Similar to the case for antiferromagnetic J, we observe that the modulus of $\langle \vec{S}_1 \vec{S}_2 \rangle(R)$ is reduced with increasing $|J|$. However, the decrease is much weaker than for antiferromagnetic J. This reduction cannot be caused by a screening of the impurity and, therefore, must have a different origin.

Figure 4(b) depicts the temperature-dependent correlation function for different ferromagnetic couplings J and for the distance $k_F R/\pi = 1.0$ (solid lines), where the RKKY

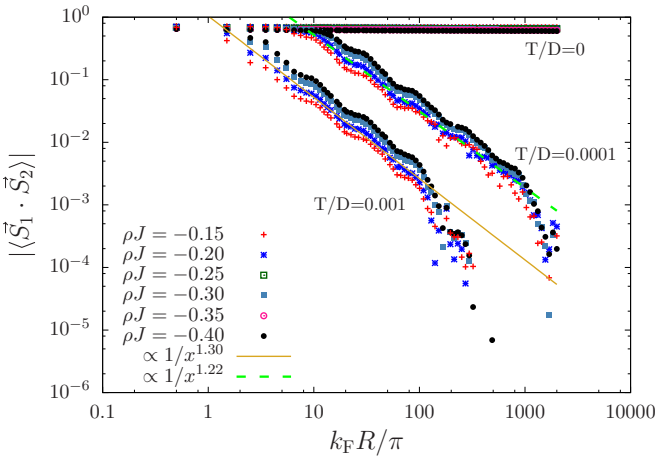

FIG. 5. The envelope of $\langle \vec{S}_1 \vec{S}_2 \rangle(R)$ for ferromagnetic couplings depicted on a double logarithmic scale. For $T = 0$, the amplitude of the correlation function remains constant for all distances. For the finite temperatures $T/D = 0.001$ and 0.0001 a power-law decay is observed when the RKKY interaction is smaller than the temperature T which turns over into an exponential decay once the length scale $\xi_T = v_F/T$ is reached.

interaction is ferromagnetic, as well as for $k_F R/\pi = 0.5$ (dashed lines), where the RKKY interaction is antiferromagnetic. For both regimes we observe (i) a reduction of the modulus of the spin-correlation function with increasing Kondo coupling J and (ii) a simultaneous increase of the crossover temperature from two uncorrelated spins at high temperatures to spin correlation in the fixed point.

For a ferromagnetic coupling $J < 0$, the effective coupling in the NRG renormalization flow is renormalized to zero $J_{\text{eff}} \to 0$ for $T \to 0$ [55]. As soon as the effective coupling is zero, a fixed point is reached and, consequently, the correlation function reaches its fixed-point value. Note, however, that the operator content of the renormalized operators is important: The larger the Kondo coupling, the smaller the fraction of the original spin that contributes to the effective spin degree of freedom that decouples from the conduction band. This is demonstrated in the inset of Fig. 4(b), which shows the fixed-point value of the correlation between an impurity spin and the spin density of the conduction electrons at the position of this impurity $\langle \vec{S}_i \vec{s}(r_i) \rangle$ for different couplings J. The correlations remain finite in the fixed point even if the effective coupling is renormalized to zero since only a part of the impurity spins decouples. The fraction of the impurity spins which remains coupled to the conduction band is the larger the larger J is.

Therefore, for a finite coupling to the conduction band the effective decoupled spins are reduced in the renormalization flow until the fixed point is reached where $J_{\text{eff}} = 0$, which is the origin of the reduction of $|\langle \vec{S}_1 \vec{S}_2 \rangle(R)|$ for FM and AFM RKKY couplings.

Note, however, that a clearly noticeable reduction of the amplitude occurs only for very large ferromagnetic couplings J.

An increasing crossover scale to the fixed point with increasing J is not observed in the SIKM and can, therefore, be ascribed to a growing RKKY interaction $\propto J^2$ since it is the only additional effect in a TIKM with ferromagnetic couplings. We have also checked that an increasing direct Heisenberg interaction between the impurity spins, as given in Eq. (3), with vanishing RKKY interaction ($R \to \infty$) has the same effect as a finite indirect RKKY interaction and also leads to an increasing crossover scale. It is already known that the RKKY interaction has a profound effect on the renormalization flow of the TIKM for antiferromagnetic Kondo couplings [56].

Figure 5 shows the envelope of the correlation function for different ferromagnetic couplings and different temperatures. As can be seen, for zero temperature $T/D = 0$, the amplitude is almost constant even for $R \to \infty$. This changes for the finite temperatures $T/D = 0.001$ and 0.0001 where a power-law decay is observed as soon as the energy scale of the RKKY interaction is smaller than the temperature. However, the finite temperature also introduces a new length scale $\xi_T = v_F/T$ beyond which the correlation function decays exponentially. The same finite temperature behavior has also been found in the SIKM for the correlation between the impurity spin and the spin density of the conduction band at a distance R from the impurity [40].

IV. REAL-TIME DYNAMICS OF THE TIKM

A. Spin-spin-correlation function after a quench

The discussion of the equilibrium properties in the previous section sets the stage for the investigation of the real-time dynamics of the time-dependent spin-spin-correlation function $\langle \vec{S}_1 \vec{S}_2 \rangle(R,t)$ after a quench of the system. We focus on antiferromagnetic Kondo couplings $J > 0$ and set the coupling of the impurities to the conduction band initially to zero $J = 0$ such that the impurities are completely decoupled from the band. At time $t = 0$ the coupling is switched on to a finite antiferromagnetic value $J > 0$ and the time-dependent behavior of $\langle \vec{S}_1 \vec{S}_2 \rangle(R,t)$ is calculated using the TD-NRG by evaluating Eq. (10).

Figure 6(a) shows $\langle \vec{S}_1 \vec{S}_2 \rangle(R,t)$ for times up to $tD = 10^6$ after such a quench for three different distances. The RKKY interaction is antiferromagnetic at the distance $k_F R/\pi = 0.51$ and ferromagnetic for the distances $k_F R/\pi = 1.00$ and 1.11. As can be seen, the correlation function behaves very differently for the three different distances, even for the two distances at which the RKKY interaction is ferromagnetic and a similar behavior is expected.

A ferromagnetic correlation emerges for small times for all distances the origin of which is caused by a ferromagnetic wave propagating through the system as we will show later. For the distance $k_F R/\pi = 0.51$, the correlation function becomes antiferromagnetic only at longer times and approaches its equilibrium value. Note the log timescale in Fig. 6(a). The equilibrium value of about $\langle \vec{S}_1 \vec{S}_2 \rangle(k_F R/\pi = 0.51) \approx -0.42$ is, however, not completely reached. For strong antiferromagnetic interactions the two impurity spins form a singlet and thus decouple from the conduction band [20,21]. Without any additional relaxation mechanism, this decoupling prevents the correlation function from reaching its equilibrium value.

The RKKY interaction has a ferromagnetic maximum for $k_F R/\pi = 1.00$. Strikingly, the correlation function changes only for short times and remains almost constant after the first

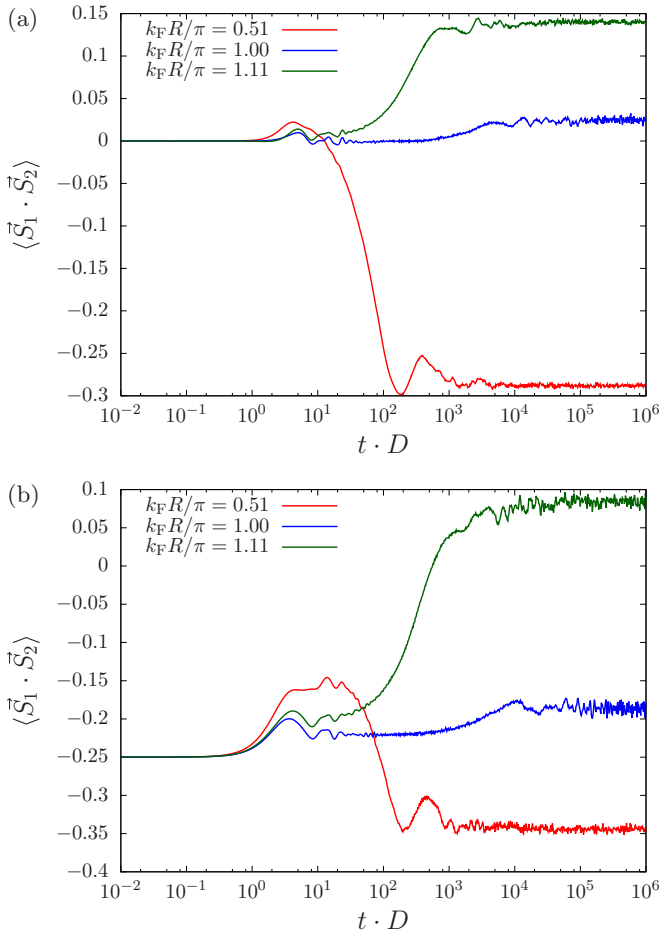

FIG. 6. (a) The long-time behavior of $\langle \vec{S}_1 \vec{S}_2 \rangle(R,t)$ after a quench in the coupling from $\rho J = 0$ to 0.2 for the three different distances $k_F R/\pi = 0.51$, 1.00, and 1.11. (b) Time dynamics of $\langle \vec{S}_1 \vec{S}_2 \rangle(R,t)$ after a quench in magnetic fields applied to the impurities from $H_1 = -H_2 = 10D$ to $H_1 = H_2 = 0$ for the same distances as in (a). NRG parameters: $\lambda = 3$, Ns = 2000, and $N_z = 32$.

ferromagnetic maximum. This surprising behavior is related to the property of the dispersion, i.e., $\epsilon(k) = \epsilon(|k|)$ [31]. At special distances $k_F R/\pi = n$, we observe that the impurity correlation function $\langle \vec{S}_1 \vec{S}_2 \rangle$ becomes a conserved quantity resulting in a fixed value for $\langle \vec{S}_1 \vec{S}_2 \rangle(R,t)$ for long times.

In order to understand this effect, one has to examine the energy dependent normalization functions between the impurities and the conduction band. For a 1D symmetric dispersion, either the even or the odd normalization function in Eq. (7) exhibits a pseudogap at the Fermi energy $\epsilon = 0$ for the distances $k_F R/\pi = n$, with $n = 0,1,2,\ldots$ (see also Fig. 1). Due to the pseudogap either $N_e(0,R) = 0$ or $N_o(0,R) = 0$ always vanishes at the Fermi energy for these special distances. This also leads to the fact that the last term of the Hamiltonian in Eq. (6) proportional to $\propto (\vec{S}_1 - \vec{S}_2) N_e(\epsilon,R) N_o(\epsilon',R)$ always vanishes on low-energy scales for the distances $k_F R/\pi = n$. This term is, however, responsible for the correlation function to smoothly evolve from a spin triplet to a singlet value or vice versa since it mixes electrons from the even and odd conduction band via impurity scattering processes. In a parity-symmetric TIKM the global parity remains conserved; however, the local impurity parity and the parity in the conduction bands may change. Once this term vanishes, the band mixing is suppressed and, therefore, the local impurity parity becomes a conserved quantity at low-energy scales. Consequently, the correlation function $\langle \vec{S}_1 \vec{S}_2 \rangle(k_F R/\pi = n,t)$ is fixed for long times due to parity symmetry.

Note that this effect is not necessarily restricted to 1D dispersions. Generally, a dispersion is needed where at certain distances either the even or the odd normalization function in Eq. (5b) vanishes or, at least, almost vanishes for small temperatures inducing a local parity conservation.

At the distance $k_F R/\pi = 1.11$ the RKKY interaction is also ferromagnetic, but the effective density of states does not exhibit a pseudogap. $\langle \vec{S}_1 \vec{S}_2 \rangle(R,t)$ approaches its ferromagnetic equilibrium value, as expected. However, the equilibrium value of $\langle \vec{S}_1 \vec{S}_2 \rangle(R) \approx 0.2$ is not completely reached.

Although qualitatively the results remain unchanged, the long-time limit of $\langle \vec{S}_1 \vec{S}_2 \rangle(R,t)$ slightly depends on the discretization parameter Λ of the NRG for times $tD > 1000$.

In order to demonstrate that the characteristic difference in the real-time dynamics of the correlation function is not only restricted to quenches in the coupling J, Fig. 6(b) shows the behavior of $\langle \vec{S}_1 \vec{S}_2 \rangle(R,t)$ after a quench in magnetic fields applied to the impurity spins from $H_1 = -H_2 = 10D$ to $H_1 = H_2 = 0$. Since the impurity spins are initially antiparallel aligned, the correlation function starts from $\langle \vec{S}_1 \vec{S}_2 \rangle(R,0) = -0.25$ at $t = 0$. As can be seen, the behavior is very similar to Fig. 6(a) such that for the distances $k_F R/\pi = 0.51$ and 1.11 the correlation function approaches its equilibrium value while for $k_F R/\pi = 1.00$ it remains close to its initial value. Also note that the initial condition with antiparallel aligned impurity spins is not parity symmetric; however, the Hamiltonian driving the time dynamics is parity symmetric and, therefore, leads to a local impurity parity conservation for the distance $k_F R/\pi = 1.00$ for long times.

B. Short-time behavior

After presenting the real-time dynamics for all timescales in the previous section, we now discuss the short-time behavior in more detail.

For zero initial correlation function $\langle \vec{S}_1 \vec{S}_2 \rangle(R,0) = 0$, the first- and second-order contributions in a perturbation expansion in J vanish so that the first nonvanishing order is $\propto J^3$ (for details see the Appendix). The impurity correlation function $\langle \vec{S}_1 \vec{S}_2 \rangle(R,t)$ calculated with the TD-NRG is depicted in Fig. 7(a) for the distance $k_F R = 0.51\pi$ and different antiferromagnetic couplings J. By rescaling the results with $1/J^3$ we demonstrate a perfect agreement with the scaling prediction of the perturbation theory which becomes exact in the limit $t \to 0$.

Around this distance a ferromagnetic correlation develops where the peak position is only dependent on the reciprocal bandwidth, and, therefore, related to the Fermi velocity. We will show below that this peak will be linearly dependent on the distance R between the impurities and is related to the information spread between the two impurities.

The inset of Fig. 7(a) shows the correlation function for the same distance and couplings plotted against the rescaled

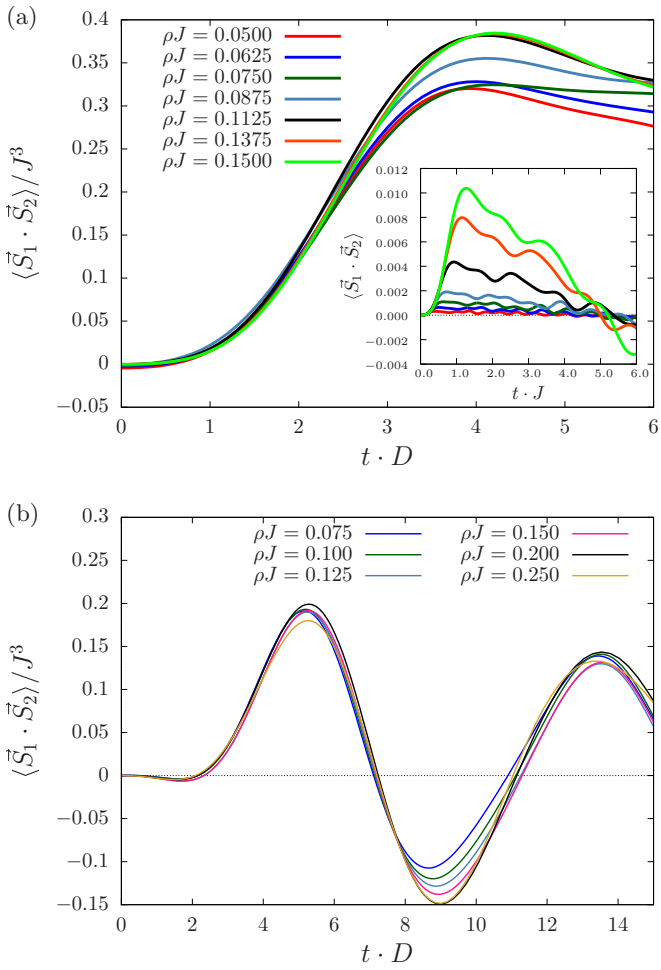

FIG. 7. (a) The short-time behavior of the spin-correlation function of the TIKM rescaled with $1/J^3$ for different couplings J and the fixed distance $k_F R = 0.51\pi$. The inset depicts $\langle \vec{S}_1 \vec{S}_2 \rangle(R,t)$ against the rescaled time tJ. Note that, due to the rescaling with J, the zero crossings from positive to negative correlations at $tJ \approx 5$ approximately coincide for all J. (b) Short-time behavior for the distance $k_F R = 1.00\pi$ and different couplings J plotted against tD. For this distance the zero crossings from positive to negative correlations at $tD \approx 7$ coincide without any rescaling of the time. NRG parameters: $\lambda = 3$, Ns $= 2000$, $N_z = 16$.

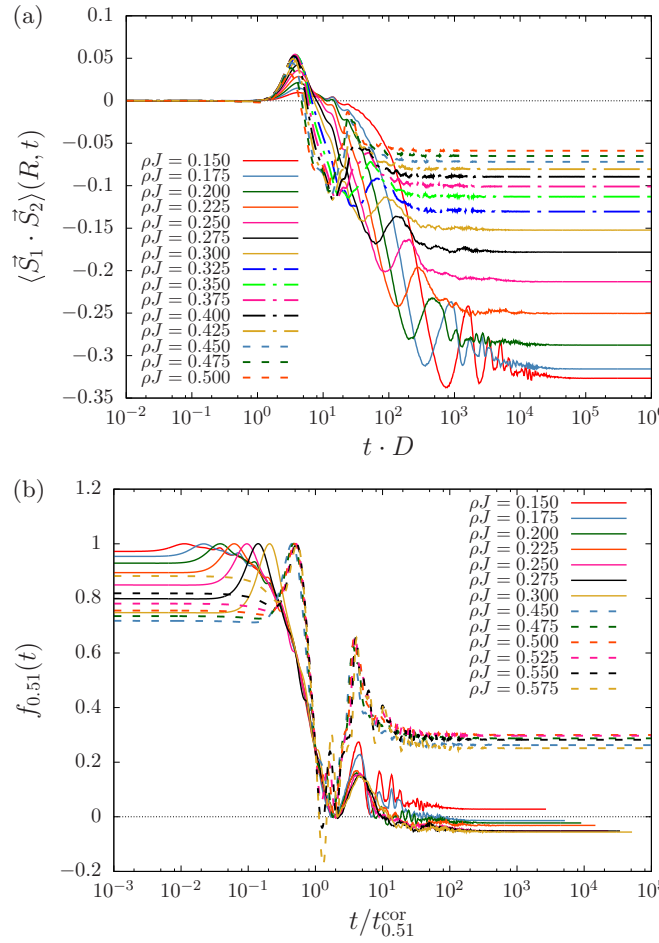

FIG. 8. (a) $\langle \vec{S}_1 \vec{S}_2 \rangle(R,t)$ for the distance $k_F R/\pi = 0.51$ and different couplings J. (b) The reduced correlation function $f_{0.51}(t)$ plotted against the rescaled time $t/t^{\mathrm{cor}}_{0.51}$. NRG parameters: $\lambda = 6$, Ns $= 2000$, $N_z = 32$, and a TD-NRG damping $\alpha = 0.2$.

time tJ. For the increase of the correlation function at times $tJ < 1$ again a universal short-time behavior is found. We can, therefore, conclude that the initial buildup of the ferromagnetic wave is proportional to $\propto (tJ)^3$.

For the distances $k_F R/\pi = n + 0.5$ the equilibrium correlation function is antiferromagnetic since the RKKY interaction reaches its largest antiferromagnetic amplitude during each oscillation cycle. However, $\langle \vec{S}_1 \vec{S}_2 \rangle(R,t)$ remains ferromagnetic for a relatively long time before it later approaches its antiferromagnetic long-time value. The inset of Fig. 7(a) reveals that the timescale of this ferromagnetic range is given by $1/J$ since for the rescaled time tJ the zero crossing from ferromagnetic to antiferromagnetic correlations is approximately $tJ \approx 5$ for all couplings J.

Figure 7(b) depicts the rescaled correlation function $\langle \vec{S}_1 \vec{S}_2 \rangle(R,t)/J^3$ for the distance $k_F R = 1.00\pi$ and different couplings. As before, a universal buildup of the ferromagnetic wave can be observed.

For this distance, however, the sign change from ferromagnetic to antiferromagnetic correlations is governed by the inverse bandwidth D that is proportional to the Fermi velocity. Because of the decoupling of one effective band, the local parity is dynamically conserved. The energy scale, and consequently also the timescale, of the decoupling are defined by the distance between the impurities and the bandwidth of the conduction band D. Therefore, due to the pseudogap formation at the distances $k_F R/\pi = n$, the relevant timescale is given by D.

C. Long-time behavior

We now turn to the investigation of the long-time behavior for different couplings J. Figure 8(a) depicts the time-dependent correlation function for the distance $k_F R/\pi = 0.51$ and different couplings J. The correlation function reaches its long-time value $\langle \vec{S}_1 \vec{S}_2 \rangle(R, t \to \infty)$ faster the stronger the coupling to the conduction band J is. Furthermore, the long-time value $|\langle \vec{S}_1 \vec{S}_2 \rangle(R, t \to \infty)|$ is reduced with increasing J,

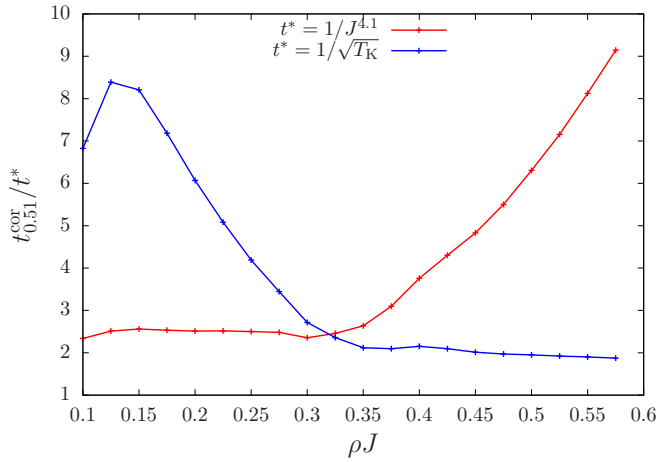

FIG. 9. The rescaled timescales $t^{cor}_{0.51} J^{4.13}$ (red line) and $t^{cor}_{0.51}\sqrt{T_K}$ (blue line) plotted against ρJ.

which coincides with the behavior observed in the equilibrium model [see Fig. 2(a)].

In order to identify a coupling dependent timescale on which the correlation function decreases and approaches its long-time value, we introduce the reduced correlation function

$$f_{0.51}(t) = \frac{\langle \vec{S}_1 \vec{S}_2 \rangle (k_F R/\pi = 0.51, t) - \langle \vec{S}_1 \vec{S}_2 \rangle_{\min}}{\langle \vec{S}_1 \vec{S}_2 \rangle_{\max} - \langle \vec{S}_1 \vec{S}_2 \rangle_{\min}}, \qquad (12)$$

where $\langle \vec{S}_1 \vec{S}_2 \rangle_{\max}$ is the maximum ferromagnetic value and $\langle \vec{S}_1 \vec{S}_2 \rangle_{\min}$ is the value of the minimum after the decrease [57]. We use this function to define the coupling dependent timescale $t^{cor}_{0.51}$ by the condition $f_{0.51}(t^{cor}_{0.51}) = 0.25$. Figure 8(b) shows the reduced correlation function $f_{0.51}(t)$ plotted versus the rescaled time $t/t^{cor}_{0.51}$ for different couplings J. We identify two distinct universal behaviors: one for small couplings $\rho J < 0.3$ (solid lines) and one for larger couplings $\rho J > 0.45$ (dashes lines). While for small couplings J the RKKY interaction drives the physics, for larger couplings the Kondo effect becomes dominant. This is in accordance with the equilibrium physics discussed before.

For small couplings the inverse timescale $1/t^{cor}_{0.51}$ shows a power-law dependence $1/t^{cor}_{0.51} \propto J^{4.1}$, which is very close to $K^2_{RKKY} \propto J^4$. In contrast, for larger couplings we observe an exponential dependency on J which agrees very well with $\sqrt{T_K}$. In order to visualize the two different dependencies of the timescale $t^{cor}_{0.51}$, Fig. 9 shows the rescaled timescale $t^{cor}_{0.51} J^{4.1}$ (red line) and $t^{cor}_{0.51}\sqrt{T_K}$ (blue line) plotted against ρJ. While for small couplings $t^{cor}_{0.51} J^{4.1}$ is almost constant, it starts to increase for $\rho J > 0.3$. On the other hand, for large couplings $\rho J > 0.4$, the curve $t^{cor}_{0.51}\sqrt{T_K}$ is almost constant. This quantifies that the crossover between an RKKY dominated physics for small J and a Kondo driven physics for large J is also found in the characteristic timescales of the nonequilibrium dynamics.

Figure 10(a) shows the long-time behavior of the correlation function for different couplings and the distance $k_F R/\pi = 1.11$. Since the RKKY interaction is ferromagnetic for this distance, the correlation function increases after the ferromagnetic wave has passed. We observe that the correlation function reaches its long-time value faster with increasing coupling

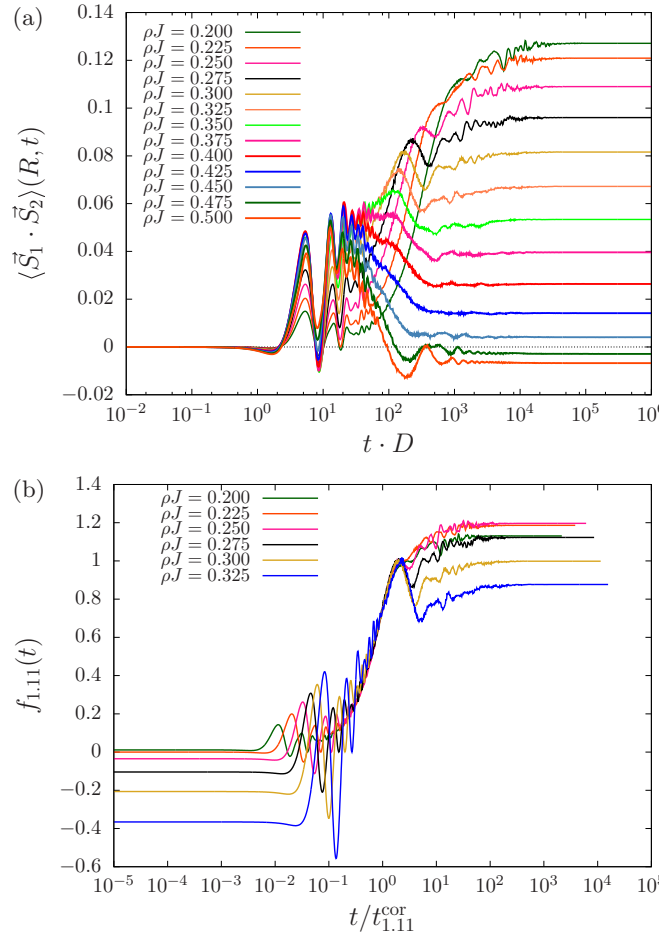

FIG. 10. (a) Time-dependent behavior of the correlation function for the distance $k_F R/\pi = 1.11$ and different couplings J. (b) The reduced correlation function $f_{1.11}(t)$ plotted against the rescaled time $t/t^{cor}_{1.11}$. NRG parameters: $\lambda = 6$, Ns $= 2000$, $N_z = 32$, and a TD-NRG damping $\alpha = 0.2$.

strength J while the long-time value $\langle \vec{S}_1 \vec{S}_2 \rangle (1.11, t \to \infty)$ is reduced.

Interestingly, for large couplings $\rho J > 0.3$ the correlation function first increases until its starts to decrease and can even reach an antiferromagnetic long-time value for couplings $\rho J \geqslant 0.475$. This behavior is in accordance with equilibrium results at low temperatures such that for the distance $k_F R/\pi = 1.11$ and couplings $\rho J \geqslant 0.475$ we also observe small antiferromagnetic correlation functions in the equilibrium NRG results. This effect has already been discussed in Sec. III A.

To extract a J dependent timescale, we again define a reduced correlation function

$$f_{1.11}(t) = \frac{\langle \vec{S}_1 \vec{S}_2 \rangle (k_F R/\pi = 1.11, t) - \langle \vec{S}_1 \vec{S}_2 \rangle_{\min}}{\langle \vec{S}_1 \vec{S}_2 \rangle_{\max} - \langle \vec{S}_1 \vec{S}_2 \rangle_{\min}}, \qquad (13)$$

where $\langle \vec{S}_1 \vec{S}_2 \rangle_{\min}$ is the value of the second minimum of $\langle \vec{S}_1 \vec{S}_2 \rangle (k_F R/\pi = 1.11, t)$ after the first ferromagnetic peak and $\langle \vec{S}_1 \vec{S}_2 \rangle_{\max}$ is the value of the maximum of the same function directly after the increase and before the correlation function starts to decrease again. Here, we modify the definition of the coupling dependent timescale to $f_{1.11}(t^{cor}_{1.11}) = 0.75$.

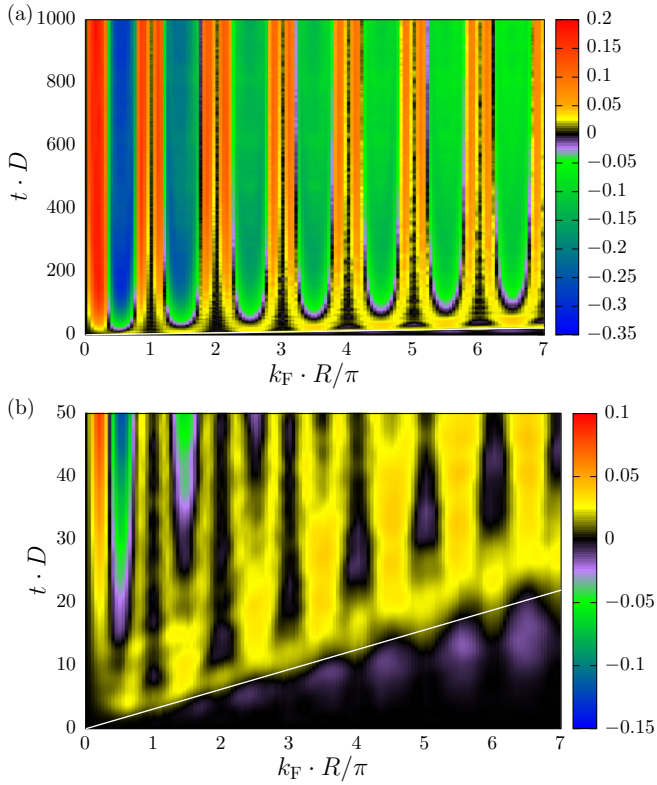

FIG. 11. (a) Time-dependent correlation function $\langle \vec{S}_1 \vec{S}_2 \rangle(R,t)$ for $\rho J = 0.2$ and a 1D dispersion. (b) The short-time behavior in more detail. The white line indicates the Fermi velocity v_F. Note that for $k_F R/\pi = n$ the correlation function does not evolve towards its equilibrium value and instead remains almost zero (vertical black lines). NRG parameters: $\lambda = 3$, Ns $= 1400$, $N_z = 4$.

The reduced correlation function $f_{1.11}(t)$ for small couplings plotted against the rescaled time $t/t_{1.11}^{\mathrm{cor}}$ is depicted in Fig. 10(b). Due to the rescaling, we find a universal behavior for the increase. The coupling dependency of the timescale is once again given by $t_{1.11}^{\mathrm{cor}} \propto J^{-4.1}$. We can, therefore, conclude that for small couplings J the timescale for the long-time behavior is the same and does not depend on whether the RKKY interaction is ferromagnetic or antiferromagnetic.

The examination of the timescales for larger couplings, however, turns out to be difficult since, as already mentioned above, the long-time behavior starts to become more complicated than a rather simple increase of the correlation function and instead starts to decrease for long times.

D. Propagation of the correlation

In this section, we investigate the propagation of correlations through the system. For that purpose, we combine the real-time dynamics calculations for different but fixed distances of the two impurities into two-dimensional plots where the horizontal axis denotes the dimensionless distance between the two impurities and the vertical axis denotes the time.

For the coupling $\rho J = 0.2$ and a 1D dispersion Fig. 11(a) depicts the correlation function for times up to $tD = 1000$ and distances up to $k_F R/\pi = 7$. For long times, $\langle \vec{S}_1 \vec{S}_2 \rangle(R,t)$ approaches its equilibrium value, and the steplike oscillations

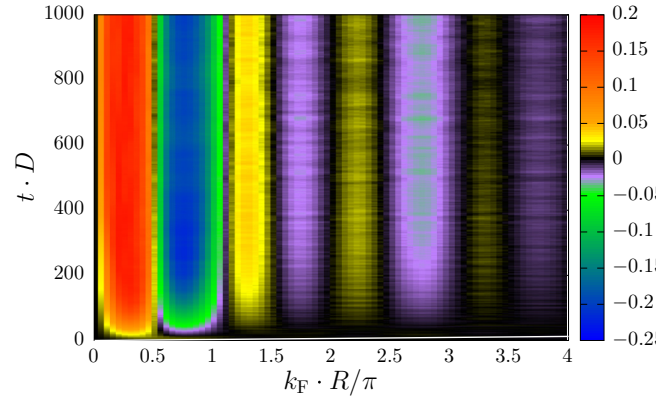

FIG. 12. Time-dependent correlation function $\langle \vec{S}_1 \vec{S}_2 \rangle(R,t)$ for a 2D linear dispersion. The white line indicates the Fermi velocity v_F. NRG parameters: $\lambda = 3$, Ns $= 1400$, $N_z = 4$.

as found in equilibrium [see Fig. 2(a)] caused by the RKKY interaction are already clearly visible for times $tD > 100$.

In the center of the ferromagnetic correlations at the magic distances $k_F R/\pi = n$, the black vertical lines indicate that the correlation function remains almost zero. At these distances the RKKY interaction is maximal ferromagnetic [see Fig. 2(a)]; however, either the even-parity or the odd-parity conduction band decouples from the problem. Therefore, the local impurity parity becomes a conserved quantity which leads to a fixed value for $\langle \vec{S}_1 \vec{S}_2 \rangle(R,t)$ as already discussed above.

Figure 11(b) depicts the same data as in Fig. 11(a) for times up to $tD = 50$ to illustrate the short-time behavior in more detail. At $k_F R/\pi = 0.5$ a ferromagnetic correlation evolves which then propagates with the Fermi velocity, indicated by the white line, through the conduction band. Directly in front of the light cone, we observe antiferromagnetic correlations at distances $k_F R/\pi = (n + 0.5)$. Such correlations outside of the light cone were also found for the correlations between the impurity spin and the spin density of the conduction band at distance R and could be traced back to the intrinsic correlations of the Fermi sea [39]. These correlations are already present before the impurities are coupled to the conduction band and are a property of the Fermi sea.

One can also see that for the distances $k_F R/\pi = (n + 0.5)$ the correlation function at first evolves towards a ferromagnetic value for a relatively long time until it later approaches its expected antiferromagnetic equilibrium value since the RKKY interaction is antiferromagnetic for these distances.

It becomes apparent that the correlation function remains almost zero for distances $k_F R/\pi = n$ after the ferromagnetic correlation wave has passed due to the local parity conservation. Note that with increasing distance R the frequency of the oscillations in $N_{e/o}^{1\mathrm{D}}(\epsilon, R)$ increases and, consequently, the width of the gap becomes narrower so that the energy scale on which the impurities see the gap decreases with $1/R$. The decreasing energy scale, on the other hand, leads to a linearly increasing timescale $\propto R$ at which $\langle \vec{S}_1 \vec{S}_2 \rangle(R,t)$ is fixed.

In order to demonstrate that the local impurity parity conservation is a special feature of certain dispersions, Fig. 12 shows the time-dependent correlation function for a linear dispersion in two dimensions. The normalization functions are given by $N_{e/o}^{2\mathrm{D}}(\epsilon, R) = \Gamma_0\{1 \pm J_0[k_F R(1 + \frac{\epsilon}{D})]\}$ in this case, with

the zeroth Bessel function $J_0(x)$ [39,40]. These hybridization functions do not exhibit a gap for any finite distance R. Note that for vanishing distance $R = 0$ the odd conduction band always decouples for all dispersions.

In two dimensions we only observe a vanishing correlation function for long times at distances separating the ferromagnetic and antiferromagnetic correlations. Unlike before, these black vertical lines are simply caused by a vanishing RKKY interaction for these distances. This is in contrast to the 1D case where $\langle \vec{S}_1 \vec{S}_2 \rangle(R,t)$ remained zero for distances where the RKKY interaction is maximal ferromagnetic. Also note that the correlation function decays faster compared to the 1D case for larger distances at large times, which is directly related to the faster decaying RKKY interaction $\propto 1/R^2$ in comparison to the $\propto 1/R$ decay for a 1D dispersion.

V. SUMMARY AND OUTLOOK

The equilibrium properties as well as real-time dynamics of the spin-correlation function between two localized spins at a distance R coupled to one conduction band via a local Heisenberg interaction J were investigated using the NRG. Since we did not add a direct exchange between the spins, spin-spin correlations can only be mediated by the indirect RKKY interaction.

In order to set the stage for the nonequilibrium dynamics after a local interaction quench, we presented the distance dependent equilibrium spin-spin-correlation function for the TIKM. There is a competition between Kondo physics and RKKY mediated singlet formation [20,21,28,29] for an AF coupling J. For a FM coupling, the distance dependent spin-spin-correlation function is only weakly coupling dependent due to reduction of J in the RG. For both signs of interactions J, the correlation function oscillates with the distance R as expected. Although the RKKY interaction varies continuously with the well-established $\cos(2k_F R)$ oscillations in one dimension, the spin-spin-correlation function $\langle \vec{S}_1 \vec{S}_2 \rangle(R,t)$ shows a steplike behavior that is reminiscent of the zero-temperature level crossing of local singlet-triplet state energies.

For distances R with generically FM RKKY interactions close to its distance dependent maximum, $\langle \vec{S}_1 \vec{S}_2 \rangle(R,t)$ clearly reveals the influence of the Kondo screening. While for $R < \xi_K$ the correlation function is ferromagnetic as expected, $\langle \vec{S}_1 \vec{S}_2 \rangle(R,t)$ can change its sign once R exceeds the Kondo correlation length ξ_K. For $R \to \infty$, two independent Kondo singlets are formed and the spin-correlation function vanishes. At finite distances and $R \gg \xi_K$, the sign of $\langle \vec{S}_1 \vec{S}_2 \rangle(R,t)$ depends on the magnitude of the potential scattering terms. The difference of these terms in the even and odd channel is related to a marginal relevant operator [24] that generates a small antiferromagnetic interaction responsible for the sign change.

For distances with purely AF RKKY interactions, at distances $k_F R/\pi = (n + 1/2)$, we found universality in R/ξ_K for the amplitude of the correlation function and a $1/R^2$ decay once the distance exceeds ξ_K, which is faster than the $1/R$ decrease of the 1D RKKY interaction: The Kondo screening of each impurity spin induces a faster decay of the correlation function.

In the case of ferromagnetic Kondo couplings $J < 0$, the amplitude remains constant even for $R \to \infty$ since the Kondo effect is absent. Only finite temperature evokes a power-law decay of the correlation function, which turns into an exponential decay once the length scale of the finite temperature ξ_T is exceeded.

The nonequilibrium dynamics of the spin-spin-correlation function after a sudden quench shows distinct behavior for short and for long times as a function of the distance. The short-time dynamics is governed by the propagation of correlations via the conduction band [39] with the Fermi velocity: A short ferromagnetic wave is propagating through the system as a consequence of the total spin conservation since locally antiferromagnetic correlations between the local spin and the local conduction electron spin density are building up. Its magnitude is defined by J^3, which can be understood from third-order perturbation theory.

We extracted the characteristic long timescale t^* for a fixed short distance reflecting the different mechanism in the real-time dynamics. While for weak coupling J the scaling $t^* \propto J^{-4}$ is related to the dominating RKKY interaction, $t^* \propto 1/\sqrt{T_K}$ reveals the dominating Kondo effect with increasing local coupling.

The most striking feature is, however, the remarkable nonequilibrium dynamics at the distances $k_F R/\pi = n$. Although the RKKY interaction reaches its periodic maxima, the correlation function only changes for short times whereas it remains constant for long times. This effect originates from the symmetry of the 1D dispersion and is caused by the fact that for these distances conduction electron states with even-parity ($n = 1,3,\ldots$) or odd-parity ($n = 0,2,\ldots$) symmetry decouple from the impurities at low temperatures. This decoupling also enforces a dynamic local parity conservation for the impurity spins which leads to a conserved value of the correlation function for long times.

This effect might be very useful for the implementation of spin qubits since the parity symmetry protects the entanglement between both spins and prevents the correlation from decaying to its equilibrium value. Usually, highly localized electrons in quantum dots are used as qubits since the localization reduces the decoherence facilitated by free-electron motion, but simultaneously increases the hyperfine interaction strength between the confined electron spin and the surrounding nuclear spins [58–61]. Making use of symmetries such as the parity to retain the entanglement might, therefore, be a way to employ more delocalized electrons and thus decrease the hyperfine interaction.

ACKNOWLEDGMENTS

B.L. thanks the Japan Society for the Promotion of Science and the Alexander von Humboldt Foundation. Parts of the computations were performed at the Supercomputer Center, Institute for Solid State Physics, University of Tokyo and the John von Neumann Institute for Computing at the Forschungszentrum Jülich under Project No. HHB00.

APPENDIX: PERTURBATIVE APPROACH FOR THE REAL-TIME CORRELATION FUNCTION

In this Appendix we will briefly present a perturbation theory to show that the lowest nonvanishing contribution to

the real-time dynamics of the correlation function is given by the third order $\propto J^3$.

For this purpose the Hamiltonian is divided into two parts $H = H_0 + H_K$ with $H_0 = \sum_{\sigma,\vec{k}} \epsilon_{\vec{k}}\, c^\dagger_{\vec{k}\sigma} c_{\vec{k}\sigma}$, the free conduction-band dispersion $\epsilon_{\vec{k}}$, and $H_K = J \sum_i \vec{S}_i \vec{s}_c(r_i)$. The time-dependent spin-correlation function $\langle \vec{S}_1 \vec{S}_2 \rangle(t)$ can be written as

$$\langle \vec{S}_1 \vec{S}_2 \rangle(t) = \mathrm{Tr}[\rho^I(t) \vec{S}_1 \vec{S}_2], \tag{A1}$$

where the index I indicates that the operator is transformed into the interaction picture, which is defined for any operator A as

$$A^I(t) = e^{iH_0 t} A e^{-iH_0 t}. \tag{A2}$$

$\vec{S}_1$ and $\vec{S}_1$ remain time independent since they commute with H_0. The von Neumann equation governs the real-time evolution of $\rho^I(t)$:

$$\partial_t \rho^I(t) = i\big[\rho^I(t), H_K^I(t)\big], \tag{A3}$$

which is integrated to

$$\rho^I(t) = \rho_0 + i \int_0^t \big[\rho_0, H_K^I(t_1)\big]\, dt_1 - \int_0^t \int_0^{t_1} \big[\big[\rho^I(t_2), H_K^I(t_2)\big], H_K^I(t_1)\big]\, dt_2\, dt_1, \tag{A4}$$

where we used the initial condition $\rho^I(0) = \rho_0$. Replacing $\rho^I(t_2)$ by ρ_0 in the second integral yields an approximate solution in $O(J^2)$. Substituting (A4) into (A1) and performing a cyclically rotation of the operators under the trace, we obtain

$$\langle \vec{S}_1 \vec{S}_2 \rangle(t) \approx \mathrm{Tr}\big[\rho_0 \vec{S}_1 \vec{S}_2\big] + i \int_0^t \mathrm{Tr}\big[\rho_0 \big[H_K^I(t_1), \vec{S}_1 \vec{S}_2\big]\big] dt_1 - \int_0^t \int_0^{t_1} \mathrm{Tr}\big[\rho_0 \big[H_K^I(t_2), \big[H_K^I(t_1), \vec{S}_1 \vec{S}_2\big]\big]\big]\, dt_2\, dt_1. \tag{A5}$$

This expression contains only expectation values that involve the initial density operator ρ_0 in which the impurity spins and the conduction electrons factorize since in H_0 the impurity spins are decoupled from the conduction band. In the absence of magnetic fields the first term vanishes, $\mathrm{Tr}[\rho_0 \vec{S}_1 \vec{S}_2] = \langle \vec{S}_1 \vec{S}_2 \rangle_0 = 0$, where the index denotes that the expectation value is taken with respect to the initial density operator ρ_0.

For the integral kernel of the first-order correction we obtain

$$\big\langle \big[H_K^I(t_1), \vec{S}_1 \vec{S}_2\big] \big\rangle_0 = -J \sum_{ijk} \epsilon^{ijk} \big(\big\langle S_1^k S_2^j \big\rangle_0 \langle s^i(r_1,t_1) \rangle_0 + \big\langle S_1^j S_2^k \big\rangle_0 \langle s^i(r_2,t_1) \rangle_0 \big) = 0, \tag{A6}$$

where the upper index indicates the spin component, ϵ^{ijk} is the Levi-Civita symbol, and $s^i(r_j,t)$ is the time-dependent spin component of the conduction-band electrons at position r_j in the interaction picture. Since all occurring expectation values vanish, also the complete first-order contribution in J vanishes.

Calculating the commutator of the second order yields only terms that are proportional to $\langle S_1^i S_2^j \rangle_0$, $\langle S_1^i S_2^j S_2^k \rangle_0$, or $\langle S_1^i S_1^j S_2^k \rangle_0$. Since all of these expectation values vanish, the second-order contribution is also zero.

In order to gain a nonvanishing contribution, a finite expectation value is needed which is, e.g., given by $\langle S_1^i S_1^i S_2^j S_2^j \rangle_0$. Such terms will occur the first time in the third-order contribution $\propto J^3$. Therefore, the lowest-order contribution to the short-time behavior of the correlation function is given by the third order. This is in accordance with the TD-NRG results that show a $\propto J^3$ dependence for short times.

[1] D. Loss and D. P. DiVincenzo, Phys. Rev. A **57**, 120 (1998).
[2] G. Burkard, D. Loss, and D. P. DiVincenzo, Phys. Rev. B **59**, 2070 (1999).
[3] B. Trauzettel, D. V. Bulaev, D. Loss, and G. Burkard, Nat. Phys. **3**, 192 (2007).
[4] A. Greilich, D. R. Yakovlev, A. Shabaev, A. L. Efros, I. A. Yugova, R. Oulton, V. Stavarache, D. Reuter, A. Wieck, and M. Bayer, Science **313**, 341 (2006).
[5] M. M. Glazov, J. Appl. Phys. **113**, 136503 (2013).
[6] I. Žutić, J. Fabian, and S. Das Sarma, Rev. Mod. Phys. **76**, 323 (2004).
[7] M. Misiorny, M. Hell, and M. R. Wegewijs, Nat. Phys. **9**, 801 (2013).
[8] W. Han, R. K. Kawakami, M. Gmitra, and J. Fabian, Nat. Nano **9**, 794 (2014).
[9] H. Johll, M. D. K. Lee, S. P. N. Ng, H. C. Kang, and E. S. Tok, Sci. Rep. **4**, 7594 (2014).
[10] O. V. Yazyev and L. Helm, Phys. Rev. B **75**, 125408 (2007).
[11] J. Bork, Y.-h. Zhang, L. Diekhoner, L. Borda, P. Simon, J. Kroha, P. Wahl, and K. Kern, Nat. Phys. **7**, 901 (2011).
[12] T. Esat, B. Lechtenberg, T. Deilmann, C. Wagner, P. Kruger, R. Temirov, M. Rohlfing, F. B. Anders, and F. S. Tautz, Nat. Phys. **12**, 867 (2016).
[13] N. Atodiresei, J. Brede, P. Lazić, V. Caciuc, G. Hoffmann, R. Wiesendanger, and S. Blügel, Phys. Rev. Lett. **105**, 066601 (2010).
[14] L. Bogani and W. Wernsdorfer, Nat. Mater. **7**, 179 (2008).
[15] S. Sanvito, Chem. Soc. Rev. **40**, 3336 (2011).
[16] W. J. M. Naber, S. Faez, and W. G. van der Wiel, J. Phys. D **40**, R205 (2007).
[17] V. A. Dediu, L. E. Hueso, I. Bergenti, and C. Taliani, Nat. Mater. **8**, 707 (2009).
[18] A. J. Drew, J. Hoppler, L. Schulz, F. L. Pratt, P. Desai, P. Shakya, T. Kreouzis, W. P. Gillin, A. Suter, N. A. Morley, V. K. Malik, A. Dubroka, K. W. Kim, H. Bouyanfif, F. Bourqui, C. Bernhard, R. Scheuermann, G. J. Nieuwenhuys, T. Prokscha, and E. Morenzoni, Nat. Mater. **8**, 109 (2009).

[19] A. Spinelli, M. Gerrits, R. Toskovic, B. Bryant, M. Ternes, and A. F. Otte, Nat. Commun. **6**, 10046 (2015).

[20] B. A. Jones, C. M. Varma, and J. W. Wilkins, Phys. Rev. Lett. **61**, 125 (1988).

[21] B. A. Jones and C. M. Varma, Phys. Rev. B **40**, 324 (1989).

[22] R. M. Fye and J. E. Hirsch, Phys. Rev. B **40**, 4780 (1989).

[23] R. M. Fye, Phys. Rev. Lett. **72**, 916 (1994).

[24] I. Affleck, A. W. W. Ludwig, and B. A. Jones, Phys. Rev. B **52**, 9528 (1995).

[25] M. A. Ruderman and C. Kittel, Phys. Rev. **96**, 99 (1954).

[26] T. Kasuya, Prog. Theor. Phys. **16**, 45 (1956).

[27] K. Yosida, Phys. Rev. **106**, 893 (1957).

[28] S. Doniach, Physica B **91**, 231 (1977).

[29] O. Sakai and Y. Shimizu, J. Phys. Soc. Jpn. **61**, 2333 (1992).

[30] J. B. Silva, W. L. C. Lima, W. C. Oliveira, J. L. N. Mello, L. N. Oliveira, and J. W. Wilkins, Phys. Rev. Lett. **76**, 275 (1996).

[31] B. Lechtenberg, F. Eickhoff, and F. B. Anders, Phys. Rev. B **96**, 041109 (2017).

[32] K. G. Wilson, Rev. Mod. Phys. **47**, 773 (1975).

[33] R. Bulla, T. A. Costi, and T. Pruschke, Rev. Mod. Phys. **80**, 395 (2008).

[34] F. B. Anders and A. Schiller, Phys. Rev. Lett. **95**, 196801 (2005).

[35] F. B. Anders and A. Schiller, Phys. Rev. B **74**, 245113 (2006).

[36] B. A. Jones and C. M. Varma, Phys. Rev. Lett. **58**, 843 (1987).

[37] K. Takasan, M. Nakagawa, and N. Kawakami, Phys. Rev. B **96**, 115120 (2017).

[38] E. H. Lieb and D. W. Robinson, Commun. Math. Phys. **28**, 251 (1972).

[39] B. Lechtenberg and F. B. Anders, Phys. Rev. B **90**, 045117 (2014).

[40] L. Borda, Phys. Rev. B **75**, 041307 (2007).

[41] C. Jayaprakash, H. R. Krishna-murthy, and J. W. Wilkins, Phys. Rev. Lett. **47**, 737 (1981).

[42] F. Eickhoff, B. Lechtenberg, and F. B. Anders, arXiv:1806.03130.

[43] H. T. M. Nghiem and T. A. Costi, Phys. Rev. B **89**, 075118 (2014).

[44] H. T. M. Nghiem and T. A. Costi, Phys. Rev. Lett. **119**, 156601 (2017).

[45] F. B. Anders, Phys. Rev. Lett. **101**, 066804 (2008).

[46] S. Schmitt and F. B. Anders, Phys. Rev. B **81**, 165106 (2010); Phys. Rev. Lett. **107**, 056801 (2011).

[47] A. Jovchev and F. B. Anders, Phys. Rev. B **87**, 195112 (2013).

[48] E. Eidelstein, A. Schiller, F. Güttge, and F. B. Anders, Phys. Rev. B **85**, 075118 (2012).

[49] F. Güttge, F. B. Anders, U. Schollwöck, E. Eidelstein, and A. Schiller, Phys. Rev. B **87**, 115115 (2013).

[50] M. Yoshida, M. A. Whitaker, and L. N. Oliveira, Phys. Rev. B **41**, 9403 (1990).

[51] A. Allerdt, C. A. Büsser, G. B. Martins, and A. E. Feiguin, Phys. Rev. B **91**, 085101 (2015).

[52] L. Zhu and C. M. Varma, arXiv:cond-mat/0607426.

[53] V. Barzykin and I. Affleck, Phys. Rev. B **57**, 432 (1998).

[54] H. Ishii, J. Low Temp. Phys. **32**, 457 (1978).

[55] P. W. Anderson, J. Phys. C **3**, 2436 (1970).

[56] A. Nejati, K. Ballmann, and J. Kroha, Phys. Rev. Lett. **118**, 117204 (2017).

[57] For large couplings $\rho J > 0.50$ a second minimum prior to the first one slowly starts to develop the value of which may even become smaller than the value of the original second minimum for very large couplings $\rho J > 0.55$. In order to achieve comparability with the curves for smaller couplings, we thus use the value of the second minimum as $\langle \vec{S}_1 \vec{S}_2 \rangle_{\min}$ for couplings $\rho J > 0.55$.

[58] R. Hanson, L. P. Kouwenhoven, J. R. Petta, S. Tarucha, and L. M. K. Vandersypen, Rev. Mod. Phys. **79**, 1217 (2007).

[59] I. A. Merkulov, A. L. Efros, and M. Rosen, Phys. Rev. B **65**, 205309 (2002).

[60] W. A. Coish and D. Loss, Phys. Rev. B **70**, 195340 (2004).

[61] J. Fischer, W. A. Coish, D. V. Bulaev, and D. Loss, Phys. Rev. B **78**, 155329 (2008).